TISSUE ENGINEERING: Part A
Volume 26, Numbers 1 and 2, 2020

DOI: 10.1089/ten.tea.2019.0051

termis
Tissue Engineering
& Regenerative Medicine
International Society

ORIGINAL ARTICLE

Amorphous Silicon Oxynitrophosphide-Coated Implants Boost Angiogenic Activity of Endothelial Cells

Felipe A. do Monte, MD, PhD,[1,2] Kamal R. Awad, MS,[3,4] Neelam Ahuja, MS,[4] Harry K.W. Kim, MD,[2,5] Pranesh Aswath, PhD,[3] Marco Brotto, PhD,[4] Venu G. Varanasi, PhD[3,4]

Lack of osteointegration is a major cause of aseptic loosening and failure of implants used in bone replacement. Implants coated with angiogenic biomaterials can improve osteointegration and potentially reduce these complications. Silicon- and phosphorus-based materials have been shown to upregulate expression of angiogenic factors and improve endothelial cell functions. In the present study, we hypothesize that implants coated with amorphous silica-based coatings in the form of silicon oxynitrophosphide (SiONP) by using plasma-enhanced chemical vapor deposition (PECVD) technique could enhance human umbilical vein endothelial cell angiogenic properties *in vitro*. The tested groups were: glass coverslip (GCS), tissue culture plate, SiON, SiONP1 (O: 7.3 at %), and SiONP2 (O: 14.2 at %) implants. The SiONP2 composition demonstrated 3.5-fold more fibronectin deposition than the GCS ($p < 0.001$). The SiONP2 group also presented a significant improvement in the capillary tubule length and thickness compared with the other groups ($p < 0.01$). At 24 h, we observed at least a twofold upregulation of vascular endothelial growth factor A, hypoxia-inducible factor-1α, angiopoietin-1, and nesprin-2, more evident in the SiONP1 and SiONP2 groups. In conclusion, the studied amorphous silica-coated implants, especially the SiONP2 composition, could enhance the endothelial cell angiogenic properties *in vitro* and may induce faster osteointegration and healing.

Keywords: amorphous silica, PECVD, SiONP, endothelial cells, angiogenesis, VEGF-A, angiopoietin-1

Impact Statement

In this study, we report for the first time the significant enhancement of human umbilical vein endothelial cell angiogenic properties (*in vitro*) by the amorphous silica-based coatings in the form of silicon oxynitrophosphide (SiONP). The SiONP2 demonstrated 3.5-fold more fibronectin deposition than the glass coverslip and presented a significant improvement in the capillary tubule length and thickness. At 24 h, SiONP reported twofold upregulation of vascular endothelial growth factor A, hypoxia-inducible factor-1α, angiopoietin-1, and nesprin-2. The studied amorphous silica-coated implants enhance the endothelial cell angiogenic properties *in vitro* and may induce faster osteointegration and healing.

Introduction

New blood vessel formation is a crucial event for adequate bone healing.[1] Large bone defects are associated with proportional vascular damage.[2] Poor vascularization results in reduced oxygen and nutrients at sites of injured tissues, which are necessary in high demand for tissues under regeneration.[3] The lack of sufficient vascularization can lead to nonunion and delayed union, requiring surgical intervention for bone replacement.[4,5] Commercially available implants, such as polyether ether ketone, TiO_2, polymethylmethacrylate, and bioceramics, have been used for this purpose.[6–9] However, the lack of osteointegration is still a problem with these materials, which can undergo some degree of loosening and failure.[10]

Studies have used bioceramic coatings to enhance osteointegration.[11–13] Frequently used materials are hydroxyapatite, which despite being the main component of natural bone, does not have osteoinductive capacity[14] as well as have

[1]Department of Bioengineering, University of Texas at Arlington, Arlington, Texas.
[2]Center for Excellence in Hip Disorders, Texas Scottish Rite Hospital, Dallas, Texas.
[3]Department of Materials Science and Engineering, University of Texas at Arlington, Arlington, Texas.
[4]Bone-Muscle Research Center, College of Nursing and Health Innovation, University of Texas at Arlington, Arlington, Texas.
[5]Department of Orthopedic Surgery, University of Texas Southwestern Medical Center at Dallas, Dallas, Texas.

poor adhesion to the substrate. Bioactive glass 45S5 (Bioglass®) is osteoinductive and osteoconductive[15]; however, the Bioglass coating process requires elevated temperatures that can create cracks and lack of efficient adhesion between the coating and underlying material leading to delamination.[16] The residual stress at the coating/metal interface due to the coupled effects of thermal expansion mismatches, and plastic deformation of the substrate/elastic recovery of the coating is the main reason for interfacial crack formation leading to delamination.[16]

However, plasma-enhanced chemical vapor deposition (PECVD) coating has remarkable advantages compared with other coating methods. This method requires a relatively low temperature ($\sim$300°C) and prevents mismatch between the coating and the substrate materials. PECVD coating can efficiently form a stable coating layer of amorphous silica on an underlying metal surface. These PECVD silica-based materials have been shown to enhance new bone formation by enhancing osteoblast differentiation and matrix deposition.[17–21] This amorphous silica-coating layer formed by Si, O, and N (SiON) is able to undergo dissolution in an *in vitro* cell-free physiological environment, and in 6 h can be rapidly released, interact with medium, and form a hydroxycarbonate apatite layer.[21]

Furthermore, the same work demonstrated that SiON-coated implants can enhance osteogenesis and biomineralization.[21] Another study using the same coating method and composition reported that SiON implants can enhance osteogenesis by upregulating superoxide dismutase 1 (SOD-1), which is a potent antioxidant enzyme that plays a role on osteogenesis, angiogenesis, and oxidative stress pathways.[17]

Moreover, these materials can induce angiogenesis in human umbilical vein endothelial cells (HUVECs) by upregulating hypoxia-inducible factor-1α (*HIF-1α*) and vascular endothelial growth factor A (*VEGF-A*).[22] Also, the previous studies explained that PECVD-coated SiON implants have a hydrophilic surface[23] with high surface energy that is directly correlated with the low contact angle (<90°) of the coating. These surface properties improved the cell attachment and proliferation.[24–27]

Other studies demonstrated that ionic phosphorus can enhance angiogenesis by upregulating *VEGF-A* in preosteoblast cell lines, metalloproteinase-2, and fibroblast growth factor-basic (bFGF) in endothelial cells.[28–30] The effect of nitrogen on HUVECs angiogenesis is unclear and sometimes ambiguous.[31] However, nitric oxide has an important role on angiogenesis due to its inhibition of angiostatin, which is an angiogenic suppressor.[32]

Moreover, it inhibits endothelial cell apoptosis, enhances endothelial cell proliferation by upregulation of *VEGF-A* and bFGF, and induces cells migration by stimulating podokinesis overexpression of integrin alpha v beta 3.[33–36]

The angiopoietin-1 (*Ang-1*) is a protein well known for playing a significant role on angiogenesis by promoting endothelial cell migration, differentiation, and survival.[37,38] Silica-based materials have been correlated with mRNA Ang-1 upregulation in HUVECs.[38] Therefore, these materials can potentially promote angiogenesis and endothelial cell viability through facilitation of Ang-1 production in the implants host environment.

Supported by the above observations, we hypothesize that a silicon oxynitrophosphide (SiONP) PECVD coating can enhance angiogenesis by facilitating endothelial cell adhesion, proliferation, migration, matrix deposition, and capillary tubule formation. Moreover, we believe that SiONP implants can overexpress angiogenic and antioxidant markers. Our initial aim was to evaluate the contact angle and cell adhesion of the surface, making a correlation between both. Following, we evaluated the effect of SiON and SiONP implants on HUVECS viability, proliferation, fibronectin deposition, cell migration, and capillary tubule formation. Finally, we measured the gene expression of angiogenic markers (*VEGF-A*, *HIF-1α*, *Ang-1*, and *nesprin-2*) and oxidative stress markers (*SOD-1*, catalase-1 [*CAT-1*], glutathione peroxidase-1, and nitric oxide sytnthase-3 [*NOS-3*]).

Materials and Methods

Study design

The materials used in this study were as follows: HUVECs, Endothelial Cell Basal Medium-2 (EBM-2), and Endothelial Cell Growth Medium-2 (EGM-2) from Lonza®; glass coverslip (GCS), tissue culture plate (TCP), and PECVD-coated amorphous silica-based implants: SiON, SiONP1 (Si = 61.8, O = 7.3, *N* = 30.5, at %), and SiONP2 (Si = 58.7, O = 14.2, *N* = 26.8, at %); Alexa Fluor 488® Phalloidin actin staining, 4′,6-Diamidine-2′-phenylindole dihydrochloride (DAPI), and Calcein-AM BD Biosciences® staining; immunostaining, anti-fibronectin (primary antibody), and mouse anti-goat with Alexa 488 (secondary antibody); Trizol®, isopropanol 100%, and ethanol 75%; RNA purification filter from Invitrogen®, GoScript™ Reverse Transcription System for cDNA conversion, and Gene expression assay from TaqMan® for angiogenic and antioxidant markers; phosphate-buffered saline (PBS), fetal bovine serum (FBS), and penicillin (10,000 units)/streptomycin (10 mg)/per milliliter (P/S) from Sigma–Aldrich.

Fluorescent images were captured using the Zeiss Axio Vert.A1 Inverted microscope. OriginPro2017, Past3, and Microsoft Excel were used for graphs and data analysis. A microplate reader was used for absorbance reading, a nanodrop was used for measuring RNA concentration, and PCR Thermo Fisher Scientific 7000 was used for cycle threshold (Ct) values on a quantitative reverse transcriptase-polymerase chain reaction (qRT-PCR). All experiments used HUVECs from passage 2 to 4, and the cells were all subcultured at least once after thawing and before experiments. Each experimental section used cells from the same passage. All PECVD-coated samples and GCS were sterilized by dry heat applied using standard bacti-cinerator inside the biosafety cabinet.

PECVD-coated amorphous silica-based implants fabrication

Four-inch diameter <100> test-grade P-type silicon wafers were acquired from NOVA Electronic Materials (Flower Mound, TX). A standard cleaning procedure was used as follows.[21] First, the silicon wafers were immersed in a piranha solution (3:1 mixture of sulfuric acid [H_2SO_4, 96%] and hydrogen peroxide [H_2O_2, 30%]) for 10 min. Second, they were removed, rinsed in deionized (DI) water, and blown with nitrogen (N_2). Third, the wafers were immersed in hydrofluoric acid to remove the native oxide layer. Finally, the wafers were rinsed in DI water for three cleaning cycles, dried with N_2 gas, then placed on 200°C hot plate for 5 min, and stored in a clean dry container.[8,9]

A TRION ORION II PECVD/LPECVD system (Trion Technology, Clearwater, FL) was used to deposit a 200 nm uniform coating of SiON and two different compositions of SiONP (Table 1). All coatings were processed at a substrate temperature (T) of 400°C (temperatures for deposition can be 200–599°C for amorphous SiONPx and SiONx films and coatings), a chamber pressure (P) of 900 mTorr (deposition pressure can be 50–2000 mTorr), an inductively coupled plasma (ICP) power of 30 W (showerhead ICP power 20–500 W), and an applied excitation frequency of 13.56 MHz(100 KHz1-GHz). The gas source and flow rates of SiON and SiONP process coatings can be seen in previous[17,21] and current[39] publications. SiONP1 and SiONP2 implants used in the presented study can be recognized by sample 3 and 4 from the latter publication.[39]

The refractive indices and thicknesses were measured using an ellipsometer at a wavelength of 632.8 nm (Gaertner LS300). The results of thickness and refractive indices were also confirmed using a reflectometer (Ocean Optics NC-UV-VIS TF Reflectometer). The elemental surface composition was verified on each PECVD-coated implant group using Energy Dispersive X-Ray Analysis (EDX) detector attached with scanning electron microscopy (SEM) (Hitachi S-3000N Variable Pressure SEM) at acceleration voltage of 12 KeV. The surface elemental composition is shown in Table 1. The SEM was also used for verifying the film thickness at 20 KeV.

Surface wettability

The tested groups were as follows: GCS, TCP, SiON, SiONP1, and SiONP2. The hydrophilicity of the surfaces was inferred from the contact angle of water. The contact angle of DI water droplets on the wafer-coated surface was measured using a sessile drop technique. For each sample, the contact angle of nine repeat drops of DI water was measured at room temperature and each coating was tested in triplicate. The images were captured using a high-speed camera (WATEC, high resolution, NAVITAR lens) synced to FTA32 Software (First Ten Angstrom).

Cell attachment

GCS of 1.5 cm diameter and TCP were used as negative and positive controls, respectively. Amorphous silica implants (SiON, SiONP1, and SiONP2) measuring 1.2×1.2 cm and GCS measuring 1.5 cm diameter were placed in a 12-well plate and 5×10^3 cells/cm^2 were seeded on the top of each surface using 100 μL of EBM-2 without FBS or other growth factors ($n = 4$ per group). We allowed the cells to attach to a specific surface for 45 min and the amount of medium was completed up to 1 mL/well. After 4 h, the surface was gently washed 2× with PBS and then fixed with 4% paraformaldehyde prepared in PBS. The cells were permeabilized with Triton X-100 (0.1%), washed with PBS, and stained with Alexa Fluor 488 for actin and DAPI for nuclei. Four fluorescent pictures were captured per group in 10× magnification, and cells were counted using ImageJ Software (NIH).

Table 1. Energy-Dispersive X-ray Spectroscopy Analysis of Atomic Surface Composition of SiON, SiONP1, and SiONP2 Coating

Sample	*Si (at %)*	*O (at %)*	*N (at %)*	*P (at %)*	*P/N*
SiON	52.5	35.1	12.3	0	0
SiONP1	61.8	7.3	30.5	0.28	0.9
SiONP2	58.7	14.2	26.8	0.27	1.0

SiONP, silicon oxynitrophosphide.

Cell viability

The cells were seeded on GCS (control for cell behavior on a silica-based surface), TCP (control for cell behavior on an optimized surface for osteoprogenitors), SiON, SiONP1, and SiONP2 surfaces in a density of 5×10^3 cells/cm^2. EBM-2 was supplemented with 0.1% FBS and 1% P/S and used as the conditioned medium.

This experiment used a 12-well plate and 6 samples per group. At 24 h, the medium was removed and added MTS assay reagent diluted five times in the cell culture medium. After 3 h, 60 μL of reagent was collected in duplicate and placed in a 96-well plate, and the absorbance was read using a spectrophotometer at 570 nm wavelength. The living cell count was collected using a standard curve acquired at the same moment in the same plate for accuracy. The data were calculated relative to the initial cell seeding number and normalized to the surface area of each group: GCS surface area (1.767 cm^2), TCP well (3.8 cm^2), PECVD-coating implants (1.44 cm^2).

Cell proliferation

Using the same cell seeding density and groups studied on the previous section ($n = 6$ per group), the cell growth relative to the positive control was evaluated after 1, 3, and 7 days. EBM-2 supplemented with 10% FBS and 1% P/S was used as the conditioned medium and changed every 48 h. The cell number was normalized according to the surface area and MTS assay was used for cell counting as mentioned in the previous section (2.4 cell viability).

Effect of eluted ions from PECVD-coated amorphous silica-based implants on HUVEC proliferation

EBM-2 was supplemented with 2% FBS +1% P/S and was used as the control for studying the eluted ions from PECVD-coated implants. Initially, EBM-2 + 1% P/S was placed in a 12-well plate with GCS, SiON, SiONP1, and SiONP2 ($n = 6$ per group) without cells for 48 h. Then, eluted ions within medium from PECVD-coated implants and medium in contact with GCS and TCP surfaces were collected from the 12-well plate and used for this experiment.

Cells were seeded (5×10^3 cells/cm^2) in a 96-well plate and allowed to attach to the well for 30 min before adding the medium with eluted ions and supplemented with 2% FBS. The cells were allowed to grow for 24 h ($n = 9$ per group) and 48 h ($n = 9$ per group). At each time point, we added 50 μL of Calcein-AM fluorescent dye for live cells. After 30 min, three pictures were captured at 5× and 10× magnifications on a Zeiss fluorescent inverted microscope per each well and used for living cells counting ($n = 3$ per group). MTS proliferation was also performed after 24 and 48 h ($n = 6$ per group).

Effect of eluted ions from PECVD-coated amorphous silica-based implants on HUVECs transwell cell migration

We used the same groups and procedures that are described in the section ''Effect of eluted ions from PECVD-coated amorphous silica-based implants on HUVECs

proliferation'' to prepare the medium before starting the cells experiment. Using 100 μL of EBM-2 + 1% P/S, 30×10^3cells were seeded on the top surface of the transwell membrane with 8 μm pore size inserted in a 24-well plate (Castor, Inc.). The plate was placed in the incubator (37°C, 5% CO_2, 90% humidity) for 30 min for adequate attachment. Then, 600 μL of medium was collected from PECVD-coated implants, and GCS were supplemented with 2% FBS and placed below the membrane ($n = 5$ per group).

After 24 h, the cells were fixed with 4% paraformaldehyde, diluted in PBS, and a sterile cotton swab was used to remove the nonmigrated cells from the upper part of the membrane. The cells were stained with DAPI, and we captured three pictures at 10× magnification using a Zeiss fluorescent inverted microscope. Cells were counted using the ImageJ Software.

Matrix deposition

The studied surfaces were: GCS, TCP, SiON, SiONP1, and SiONP2 ($n = 6$ per group). We seeded 5×10^3 cells/cm^2 using a 12-well plate. The GCS and PECVD-coated implants dimensions were the same as used for the cell attachment, viability, and proliferation. EGM-2 + 10% FBS +1%P/S was used on the positive control (TCP), and EGM-2 + 2% FBS +1% P/S was used for the negative control (GCS) and on amorphous silica implants (SiON, SiONP1, and SiONP2).

The cells were allowed to grow for 5 days. Then, the surfaces were blocked with 1% bovine serum albumin prepared in PBS solution, exposed to the primary antibody anti-fibronectin, and to the secondary antibody (mouse anti-goat IgG Alexa Fluor™ 488) labeled with Alexa 488. We captured three pictures per sample using a Zeiss fluorescent inverted microscope at 10× and 20× magnifications.

Finally, the ImageJ Software was used to measure the percentage of area occupied by fibronectin.

Capillary tubule formation on Matrigel® assay

Using a 12-well plate, the cells were seeded on GCS, TCP, SiON, SiONP1, and SiONP2 ($n = 4$ per group) at a density of 60× cell/cm^2 per well. Before starting the experiment, pipette tips and well plates were placed in a −20°C freezer for 1 h and the Matrigel thawed overnight at 4°C. First, a 12-well plate was placed on an ice block inside the cell culture hood and 200 μL of Matrigel was placed on top of GCS, TCP, or amorphous silica implants. Second, the plates with Matrigel were placed inside the incubator (37°C, 5% CO_2, 90% humidity) for 30 min. Third, the cells were seeded, and the experiment ran for 6 h. Finally, Calcein-AM 3 μM was diluted in EBM-2, the medium was carefully aspirated, and the new medium with Calcein-AM was added. After 30 min, we captured three pictures per well at 10× magnification and used the ImageJ Software for the quantification of total tubule length and tubule thickness.

Quantitative reverse transcriptase–polymerase chain reaction

In this experiment, 20×10^4 cells per sample were seeded ($n = 4$ per group) and EBM +5% FBS was used as the conditioned medium for all the groups (TCP, SiON, SiONP1, and SiONP2). Initially, we seeded the cells on studied surfaces using 100 μL of medium. After 30 min in the incubator, the total medium was filled up to 1 mL per well. At each time point, 1 mL of Trizol was added inside each well and mixed. The cell lysate with RNA was collected and placed in a 1.5 mL centrifuge tube and 100 μL of chloroform was added into each tube, mixed, left for 5 min, and centrifuged at 13,000 rpm for 15 min. After centrifugation, ~300 μL of the transparent top layer containing RNA was collected without disturbing the bottom layers (DNA and proteins) and placed in a new 1.5 mL centrifuge tube.

Five hundred microliters of isopropanol 100% was added to the new tubes for RNA precipitation and the samples were centrifuged at 13,000 rpm for 10 min. The isopropanol was removed without disturbing the RNA pellet, and 1 mL ethanol 70% was placed inside the tubes and centrifuged at 10,000 rpm for 5 min. The ethanol was carefully removed without disturbing the RNA pellet, and the tubes were kept open at room temperature for 10 min for ethanol evaporation. At the end, we added 25 μL of RNA-free water in each tube for RNA resuspension. The RNA concentration was measured using a micro-volume UV-vis spectrophotometer (Nano Drop 2000c; Thermo Fisher Scientific, Inc., Watham, MA), and all samples were diluted to 100 ng/μL during cDNA conversion using the GoScript Reverse Transcription System.

Gene expression assays (TaqMan) were acquired from ThermoFisher Scientific and prepared in a 20 μL reaction using a 96-microplate following step-by-step company protocol. We used Applied Biosystems® 7500 Real-Time PCR Systems with a standard TaqMan set up, 50 cycles for a Ct values measurements, and the samples were analyzed in duplicate. We used the delta-delta Ct method for calculations. The results were shown relative to the housekeeping gene and compared with the control. The housekeeping gene was *18S*, and the studied genes were: *VEGF-A*, *HIF-1α*, *Ang-1*, *nesprin-2*, *SOD-1*, *Cat-1*, and *NOS-3* (Table 2).

Statistics

The data are shown as the mean ± standard deviation. An unpaired *T*-test for data from two groups or one-way analysis of variance with *post hoc* Tukey's pairwise for data from groups of three or more was used to compare and detect significant differences, considering a p-value of <0.05. Sample size was determined based on the number of groups and standard deviation from a pilot study and previous publications,[17,40,41] and G*Power 3 version 3.0.5 Statistical Software was used for calculations. A confidence interval of 95% and a statistical power of 80% for all required calculations were considered. A Pearson correlation coefficient was considered

Table 2. Gene and Specific TagMan Assay Identification

Gene	*Assay identification*
VEGF-A	Hs00900055_m1
HIF-1α	Hs00153153_m1
Ang-1	Hs00919202_m1
Nesprin-2 (*SYNE2*)	Hs00794881_m1
SOD-1	Hs00533490_m1
Cat-1 (*CAT*)	Hs00156308_m1
e-NOS (*NOS3*)	Hs01574665_m1

CAT-1, catalase-1; *HIF-1α*, hypoxia-inducible factor-1α; *SOD-1*, superoxide dismutase 1; *VEGF-A*, vascular endothelial growth factor A.

as high/strong (0.5–1), moderate/medium (0.3–0.49), or low/small (≤0.29). Positive values were considered as direct and negative values as inverse correlation.

Results

Surface wettability and surface composition

The results of surface wettability for all the tested groups are presented in Figure 1. Figure 1A shows the contact angle measured on GCS (64.81 ± 6.26°), TCP (50.04 ± 3.32°), SiON (40.31 ± 2.92°), SiONP1 (47.39 ± 1.01°), and SiONP2 (32.47 ± 1.73°) surfaces. SiONP2 surface shows the lowest contact angle compared with others. However, GCS presented the highest contact angle compared with other groups ($p < 0.001$), which is more than twofold higher compared with the SiONP2 implant ($p < 0.001$).

Table 1 shows the surface composition analysis by EDX of the PECVD different coatings (200 nm). All the coatings have a comparable Si (at %) concentration, but SiON (35.1 at %) has highest oxygen concentration compared with SiONP1 (7.3 at %) and SiONP2 (14.2 at %). Also, the nitrogen concentration was lowest for SiON (12.3 at %) compared with SiONP1 (30.5 at %) and SiONP2 (26.8 at %). Both SiONP1 (0.28 at %) and SiONP2 (0.27 at %) show a comparable concentration of phosphorous.

Cell attachment and morphology and correlation with wettability

The results of cell attachment in Figure 1A and B revealed that the GCS group had the lowest attached cell count of all the groups ($p < 0.001$), indicated by at least threefold less cells than TCP, SiON, and SiONP1, and fivefold less cells than SiONP2. SiONP2 presented almost twofold more attached cells than TCP, SiON, and SiONP1 surfaces ($p < 0.001$). SiON surface presented a significant number of cell attachment compared with SiONP1 ($p < 0.05$).

The number of cells attached on the studied surfaces was correlated with the contact angle for each surface, and we observed a significant strong inverse correlation between the parameters ($r = -0.95$, $p = 0.0098$), as shown in Figure 1C and D.

Cell viability and proliferation

No cytotoxic effects were observed to HUVECs under minimal survival conditions of EBM-2 and 0.1% FBS on any surface. We observed that HUVECs exposed to the SiONP groups (SiONP1 and SiONP2) had a significant improvement in cell number relative to both positive (TCP) and negative controls (GCS), as presented in Figure 2A.

The study of cell growth relative to TCP (positive control) demonstrated that SiONP2 implants presented a significant enhancement on cells growth among the groups after 3 ($p < 0.01$) and 7 days ($p < 0.001$). All amorphous silica implants presented at least twofold more cells than the TCP ($p < 0.001$) and fourfold more than the GCS ($p < 0.001$) after 7 days of culture (Fig. 2B).

Effect of eluted ions on HUVEC proliferation

After 24 h of the elution experiment, eluted ions from PECVD-coated amorphous silica surfaces significantly enhanced cell growth compared with control (EBM-2 + 2% FBS,

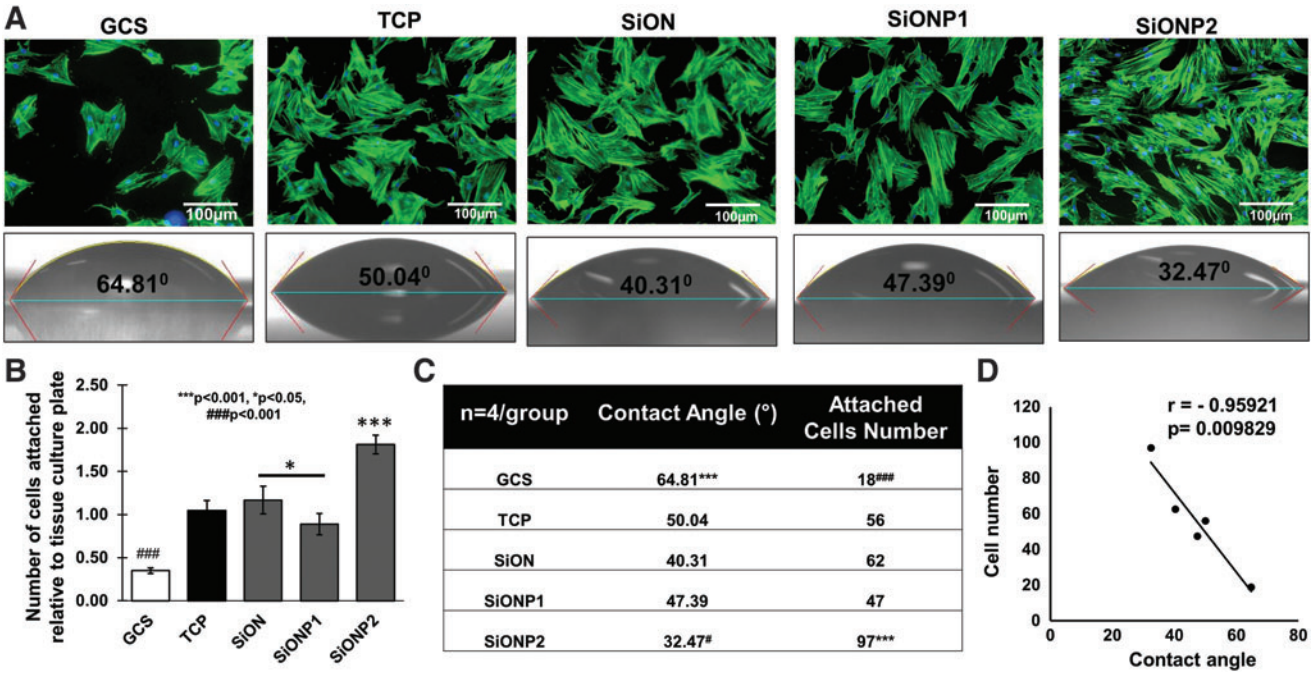

FIG. 1. Cell attachment and contact angle. **(A)** Actin and nuclei fluorescent staining showing HUVECs attached to studied surfaces 4 h after seeding in EBM-2 without FBS (*top*). Scale bar = 100 µm. Contact angle/surface wettability (*bottom*). **(B)** Bar graph shows the cell attached number relative to TCP. **(C)** Table shows the average of contact angle and cell attachment number. ANOVA, *$p < 0.05$, ***$p < 0.001$, ###$p < 0.001$, #$p < 0.05$ indicate statistical significance, $n = 4$ per group. **(D)** Correlation cell attachment number and contact angle. Correlation test of Pearson, $p < 0.05$ indicates statistical significance, $r < 0$ indicates inverse correlation. ANOVA, analysis of variance; EBM-2, endothelial cell basal media-2; FBS, fetal bovine serum; GCS, glass coverslip; HUVEC, human umbilical vein endothelial cell; TCP, tissue culture plate. Color images are available online.

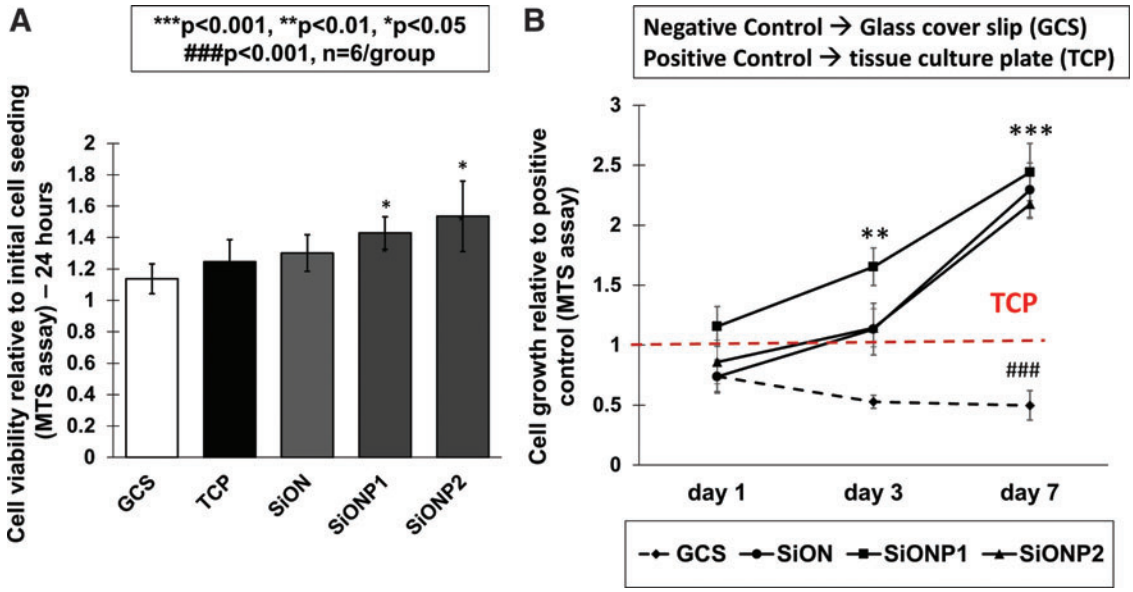

FIG. 2. Cell viability and proliferation. **(A)** Graph shows cell viability after 24 h (MTS assay). **(B)** Chart shows cell growth after 1, 3, and 7 days (MTS assay). ANOVA, ***$p<0.001$, **$p<0.01$, *$p<0.05$, ###$p<0.001$ indicate statistical significance, $n=6$ per group. Color images are available online.

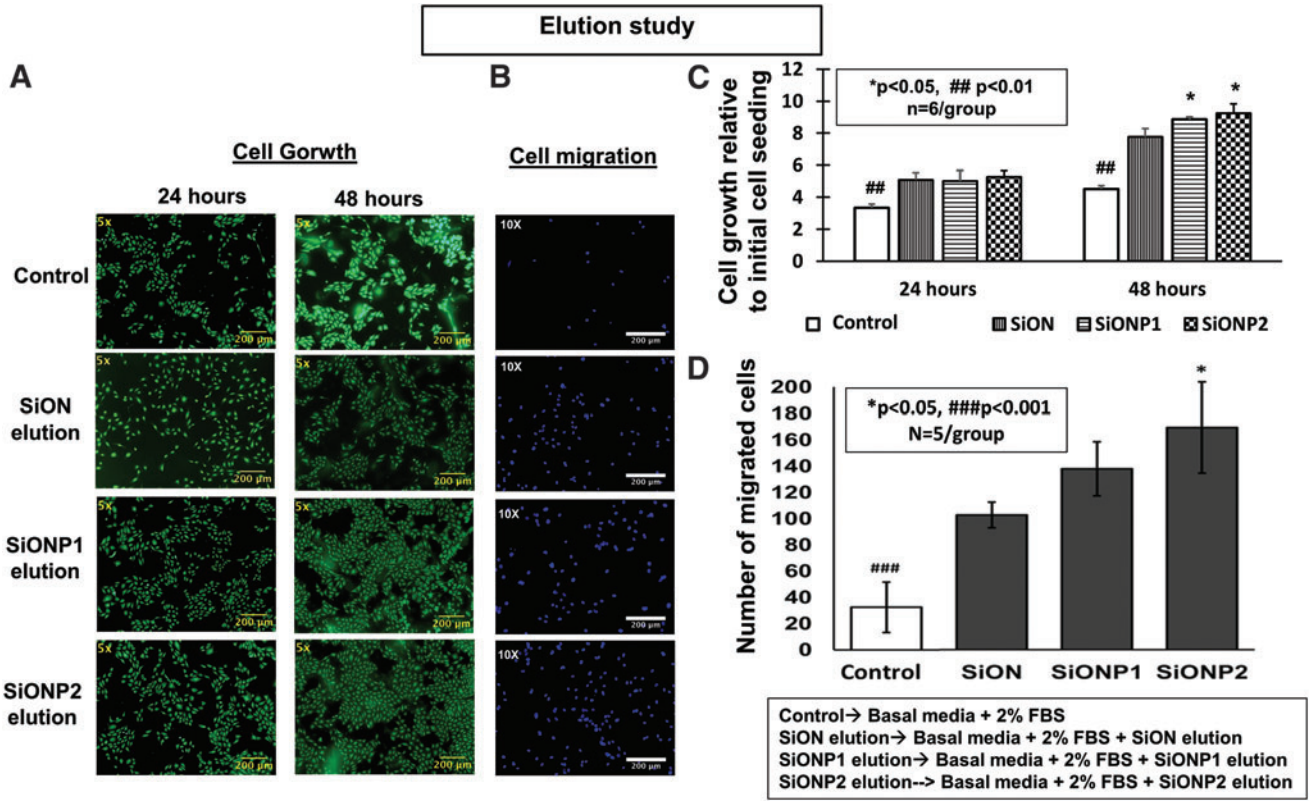

FIG. 3. **(A)** Effect of elution from amorphous silica PECVD-coating scaffolds on HUVEC proliferation. Pictures after Calcein-AM staining (24 and 48 h). Scale bar = 200 µm **(B)** Effect of elution from PECVD-coating implants on HUVECs membrane transwell migration (24 hours). **(B)** Fluorescent pictures of nuclei fluorescent staining. Scale bar = 200 µm. **(C, D)** Bar graphs show the number of growth and migrated cells. ANOVA, *$p<0.05$, ##$p<0.01$, ###$p<0.001$ indicate statistical significance. PECVD, plasma-enhanced chemical vapor deposition. Color images are available online.

$p<0.01$). Fluorescent images show representative views of each studied group (Fig. 3A). After 48 h, the SiONP groups presented twofold more cells than the GCS (control) ($p<0.01$) (Fig. 3C).

Transwell membrane cell migration

The ions released from implants on conditioned medium were tested on HUVECs after 24 h and compared with control (EBM-2 + 2% FBS). The only difference between medium collected from the control and PECVD-coated implants was the presence of ions released from the SiON, SiONP1, and SiONP2 groups. All amorphous silica implants coated by PECVD method presented a significant improvement on cell migration compared with EBM-2 + 2% FBS ($p<0.001$), showing at least threefold more cells. Representative images of DAPI fluorescent staining are shown in Figure 3B and related with bar graph in Figure 3D.

Matrix deposition

The surfaces were tested for fibronectin deposition after 5 days in EBM-2 + 2% FBS on GCS (negative control) and PECVD-coated amorphous silica groups and 10% FBS on TCP (positive control). The SiON and SiONP groups presented a significant enrichment in fibronectin deposition compared with the GCS ($p<0.01$). SiONP2 implants presented the most significant enhancement among all studied groups ($p<0.001$). The SiONP groups showed a significant improvement compared with SiON ($p<0.01$) (Fig. 4K).

Fluorescent images demonstrated that the PECVD-coated amorphous silica implants presented fibronectin deposition forming a dense tubular shape network (Fig. 4E–J). The GCS group formed a low-density tubule network structure and the TCP group formed a relatively dense fibronectin deposition with poor tubular network structure (Fig. 4A–D). High-density and dense tubular network structure for fibronectin deposition indicates enhanced vascular tubule network formation.

Capillary tube formation assay

After analysis on the ImageJ Software plugin (Angiogenesis Analyzer), the SiON, SiONP1, and SiONP2 groups exhibited a substantial enhancement on the tubule length compared with the GCS ($p<0.05$). The most significant difference was observed on SiONP2 ($p<0.01$), which presented more than twofold tubule length compared with the GCS. The SiONP groups presented twofold more tubule thickness among all studied groups ($p<0.001$) (Fig. 5).

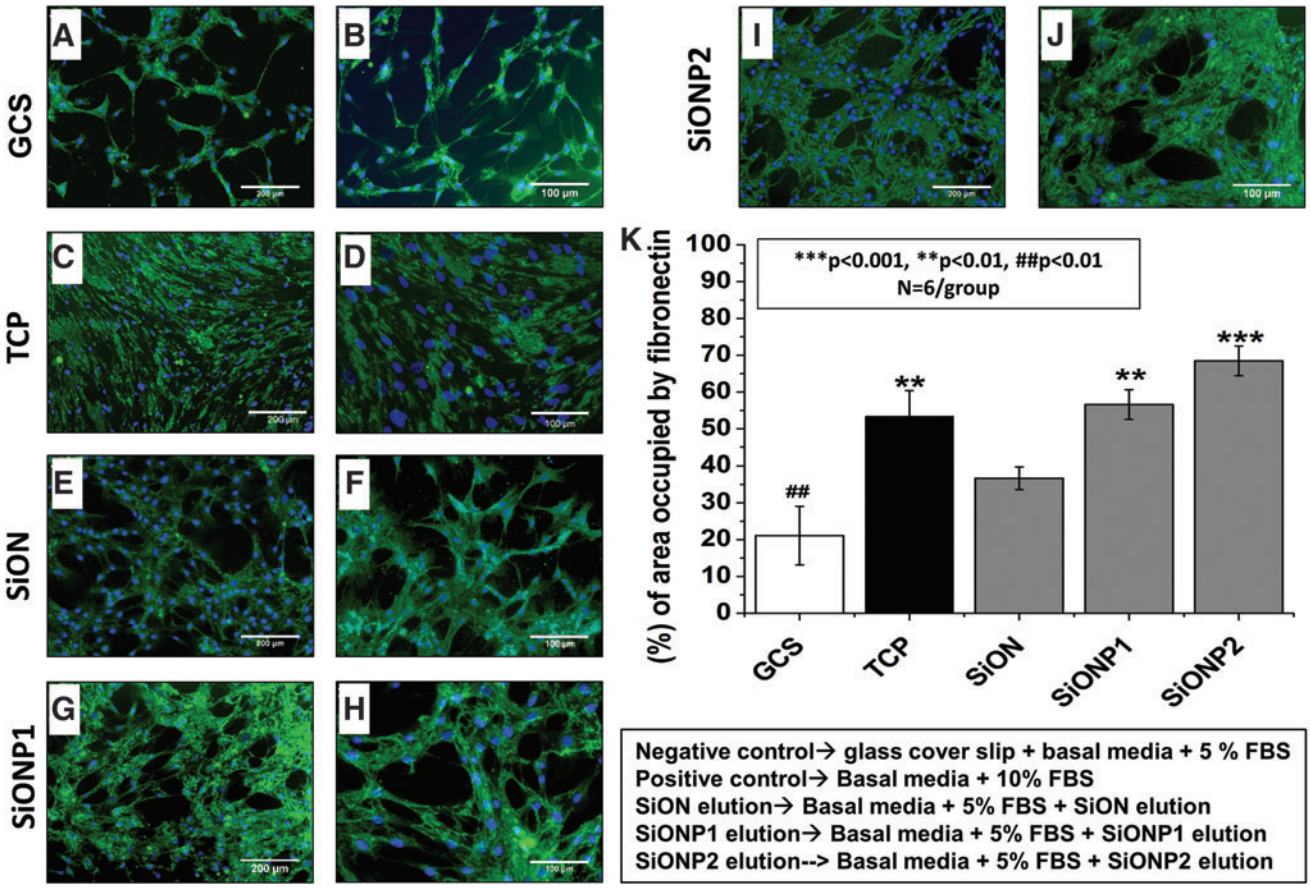

FIG. 4. HUVECs matrix deposition after 5 days in cell culture. **(A-J)** Fluorescent pictures of fibronectin immunostaining (*green*) and nuclei staining (*blue*). **(A, C, E, G, and I)** Were captured in 10× view, scale bar = 200 μm. **(B, D, F, H and J)** were captured in 20× view, scale bar = 100 μm. Graph shows percentage of area occupied by fibronectin **(K)**. ANOVA, ***$p<0.001$, **$p<0.01$, ##$p<0.01$ indicate statistical significance, $n=6$ per group. Color images are available online.

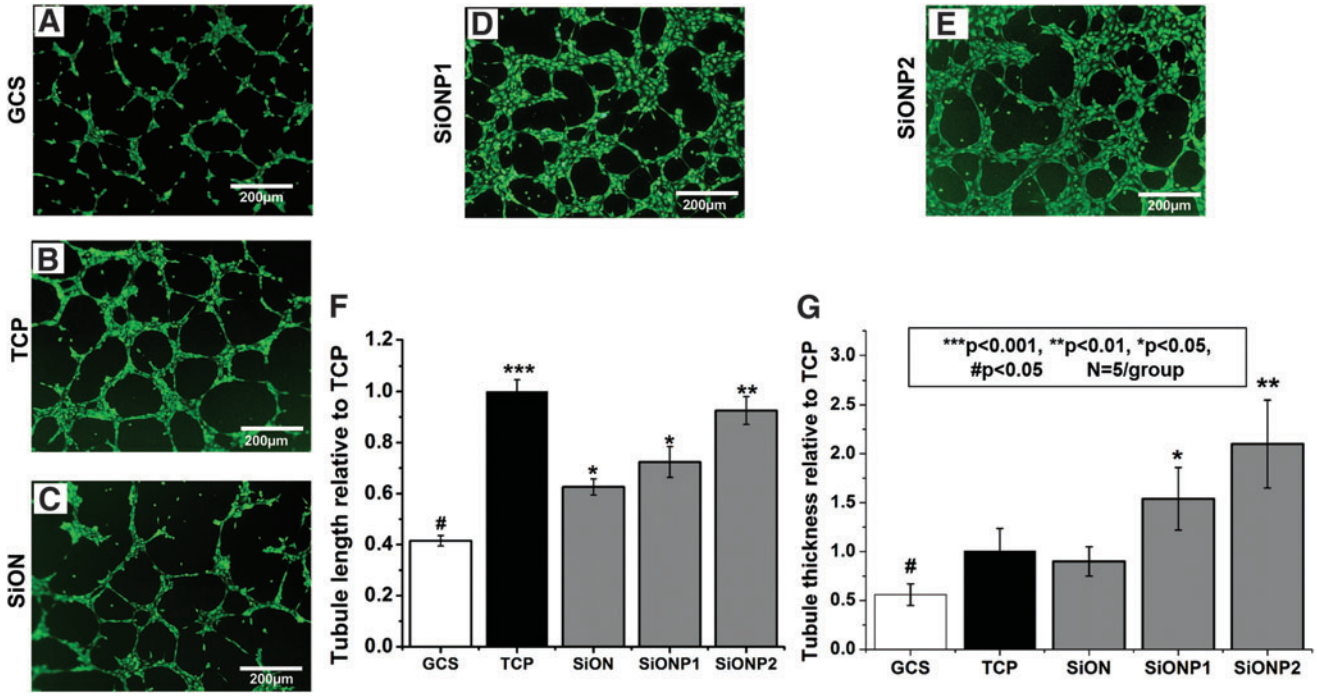

FIG. 5. Capillary tubule formation 6 h after culture on bed of Matrigel®. **(A–E)** Fluorescent images captured after Calcein-AM staining. Scale bar = 200 μm. **(F)** Bar graph shows tubule length relative to TCP (positive control). **(G)** Bar graph shows tubules thickness relative to TCP (positive control). ANOVA, $***p<0.001$, $**p<0.01$, $*p<0.05$, $\#p<0.05$ indicate statistical significance, $n=4$ per group. Color images are available online.

Quantitative reverse transcriptase–polymerase chain reaction

Gene expression of angiogenic markers. *VEGF-A*, *HIF-1α*, *Ang-1*, and *Nes-2* gene expression was measured after 24 and 48 h. After 24 h, all PECVD-coated amorphous silica implants presented at least twofold more expression than the control group ($p<0.05$) (Fig. 6A). After 72 h, SiONP implants expressed at least twofold more angiogenic markers than the control ($p<0.05$), and SiONP2 showed a remarkable heightening ($p<0.01$), especially fivefold expression of *Nes-2* (Fig. 6B).

Gene expression of antioxidant enzymes. *SOD-1*, *Cat-1*, and *NOS-3* demonstrated to be significantly upregulated at 24 h in SiON, SiONP1, and SiONP2 ($p<0.05$) and at 72 h in SiONP1 and SiONP2 ($p<0.05$). At 24 h, *Cat-1* was at least twofold enhanced in PECVD-coated amorphous silica groups compared with the control ($p<0.01$), and SiONP2 enhanced *Cat-1* expression at least threefold more than the control ($p<0.001$) (Fig. 6C). At 48 h, SiONP2 was 4.5-fold greater for *NOS-3* expression ($p<0.001$) and 2.5-fold greater for *SOD1* expression ($p<0.01$) (Fig. 6D).

Discussion

In the present study, we tested the hypothesis that PECVD-coated amorphous silica implants formed by silicon, oxygen, nitrogen, and phosphorus can boost angiogenesis in endothelial cells under normal/physiological *in vitro* condition. We verified that amorphous silica-coated implants can enhance the angiogenic properties of HUVECs by improving cell adhesion, proliferation, migration, capillary tubule formation (as summarized in Table 3), and gene expression of angiogenic indicators.

In the present study and based on the EDX results, SiONP1-coated implants have the highest nitrogen percentage compared with SiON and SiONP2 implants. Our previous study indicated that the surface wettability decreased as the nitrogen percentage increased and otherwise with the oxygen percentage in the PECVD coatings that lead to N-H bonds formation rather than the hydrophilic Si-O bonds.[23] This observation can explain the high contact angle (low wettability) of SiONP1 implants that have the highest nitrogen content compared with SiON and SiONP2.

By comparing the SiONP1 and SiONP2 implants, the N-content decrease and O-content increase from SiONP1 to SiONP2 can explain the decrease in contact angle and the high surface wettability of SiONP2. Thus, SiONP2 implants reported the lowest contact angle and the highest surface energy/wettability compared with all the tested groups. It is well known that surfaces with lower contact angles (<90°) present high surface energy and wettability (hydrophilicity) that lead to improved cells attachment and proliferation within the first 6 h of the cell culture.[23,27,42,43]

In the present study, once cells were exposed for a short period of time to the studied surfaces (4 h) with no FBS or growth factors, the HUVECs attachment was significantly enhanced on the SiONP2 surface (Fig. 1A, B), and this observation was strongly inversely correlated with the contact angle (Fig. 1C, D). These findings verify that the wettability and surface energy play a crucial role in the cell attachment within the first 4 h of implants/cells contact.

As expected, the materials synthesized in our experiment did not present cytotoxic effects on HUVECs under

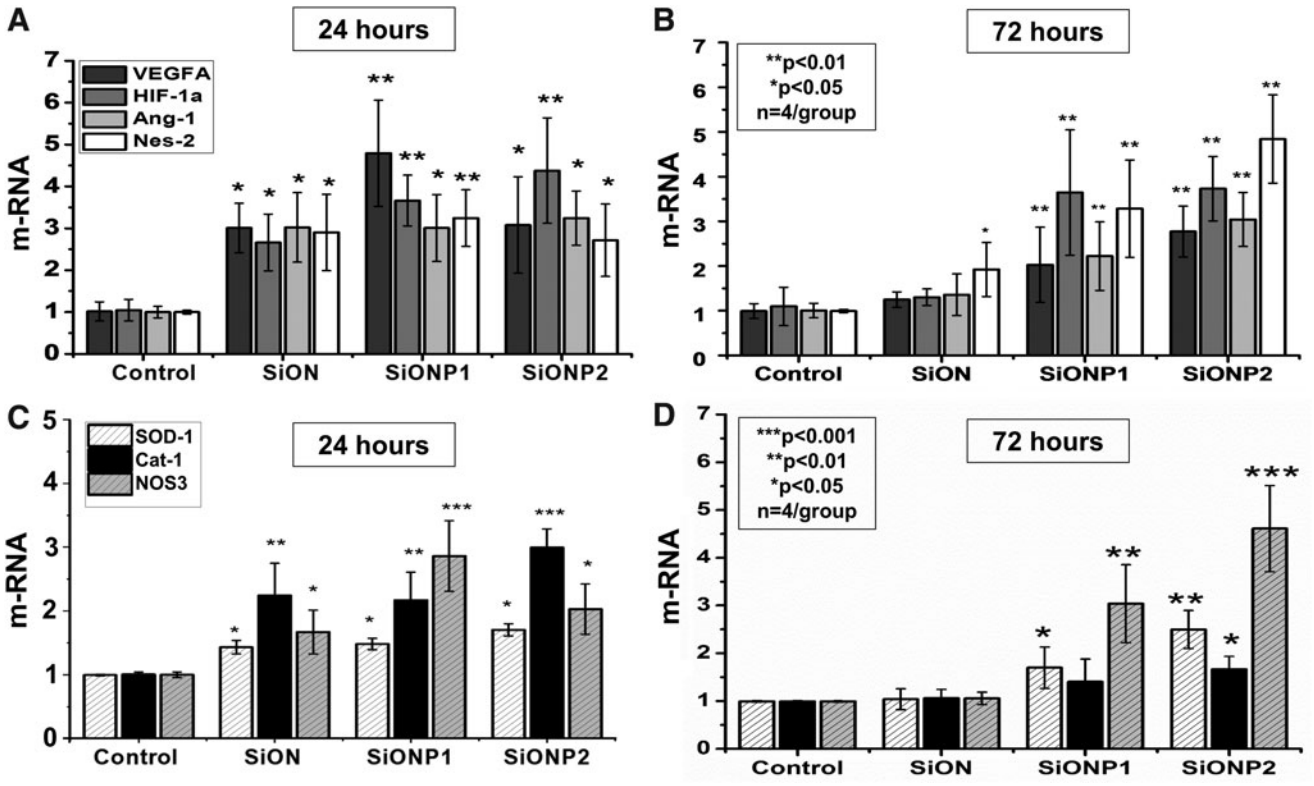

FIG. 6. Gene expression angiogenic markers relative to *18S* as compared with control at 24 h **(A)** and 72 h **(B)**. Gene expression antioxidant enzymes relative to *18S* compared with control at 24 h **(C)** and 72 h **(D)**. ***$p < 0.001$, **$p < 0.01$, *$p < 0.05$ indicate statistical significance, $n = 4$ per group. CONTROL, endothelial cell basal medium supplemented with 2% FBS on TCP; *VEGF-A*, vascular endothelia growth factor A; *HIF-1α*, hypoxia-inducible growth factor-1α; *Ang-1*, angiopoietin-1; *Nes-2*, nesprin-2.

minimum FBS condition (Fig. 2A). Relative cell growth, indirectly evaluated by the MTS proliferation assay, verified that during the studied time frame all PECVD-coated amorphous silica implant groups presented a significant improvement in cell growth compared with GCS and TCP. Especially, after 7 days, SiON, SiONP1, and SiONP2 presented at least twofold more cells than the positive control (TCP) (Fig. 2B).

The significant improvement in cell growth on the amorphous silica-based implants can be attributed to the surface chemistry of these coatings. Due to its amorphous nature, these PECVD coatings released Si, N, and P ions that enhance the cell proliferation compared with the positive and negative controls. These findings corroborate previous publications where ionic silicon-based materials enhanced endothelial cell proliferation due to the effect of the released Si ion that stimulate endothelial cell functions, such as cell migration, chemotactic homing, and tubular networking.[39,44]

Currently, we reported the dissolution of the amorphous silica-based coatings produced by the PECVD technique,

TABLE 3. SUMMARIZE THE STUDY RESULTS

	GCS	*TCP*	*SiON*	*SiONP1*	*SiONP2*
Cell growth relative to initial cell seeding (24 h) ($n = 6$ per group)	3.3 ± 0.2	N/A	5.1 ± 0.5*	5 ± 0.7*	5.2 ± 0.4*
Cell growth relative to initial cell seeding (48 h) ($n = 6$ per group)	4.5 ± 0.2	N/A	7.8 ± 0.5**	8.9 ± 0.1**	9.2 ± 0.6**
No. of migrated cells ($n = 5$ per group)	32 ± 19	N/A	97 ± 9***	131 ± 19***	160 ± 32***
Area occupied by fibronectin (%) ($n = 6$ per group)	21.1 ± 8	53.3 ± 7	36.7 ± 3	56.5 ± 4**	68.4 ± 4***
Total tubule length relative to TCP ($n = 4$ per group)	0.41 ± 0.02#	1.0 ± 0.04	0.62 ± 0.03#	0.7 ± 0.06#	0.92 ± 0.05
Total tubule thickness relative to TCP ($n = 4$ per group)	0.5 ± 0.11#	1.0 ± 0.23	0.9 ± 0.15	1.54 ± 0.32*	2.1 ± 0.45**

ANOVA, *$p < 0.05$, **$p < 0.01$, ***$p < 0.001$, #$p < 0.05$ indicate statistical significance. ANOVA, analysis of variance; GCS, glass coverslip; TCP, tissue culture plate; N/A, not applicable.

the same method used in Ilyas *et al.*'s study.[39] In that study, inductively coupled plasma optical emission spectrometry analysis confirmed the presence of Si and P ions released from SiONP coatings produced by the PECVD technique. It also revealed that ionic silicon released from the amorphous silica coating in cell culture medium has a sustained release from 30 min to 8 days.[39]

Based on the latter observation that surface chemistry and released ions can have some effect on endothelial cell proliferation, we designed an experiment utilizing the eluted ions from studied surfaces and evaluated the cells proliferation by MTS assay and Calcein-AM staining at 24 and 48 h.

Our findings demonstrated that ions released from coated materials, mainly Si and N, could induce a significant improvement in endothelial cell growth after 24 and 48 h. The FBS concentration used on the eluted material from SiON, SiONP1, and SiONP2 was the same used on the control (2% FBS), the eluted ions from all silica implants showed twofold more cells at 24 h, and especially SiONP groups presented twofold more cells at 48 h. We believe that the enhancement on cell proliferation at 48 h on elution experiment (Fig. 3A, C) could be due to P incorporation or higher Si and N content within the medium collected from the SiONP1 and SiONP2 groups. Previous studies correlated the presence of ionic Si and P with an enhancement on endothelial cell angiogenic properties.[30,31,44–46]

The role of N on endothelial cell angiogenesis is still unclear, and the direct effect has been related to N reacting with oxygen forming NO.[32]

The SiON, SiONP1, and SiONP2 coatings showed a significant enhancement on cell migration compared with control (EBM +2% FBS) (Fig. 3B, D), showing that the ionic content released from implants coated with amorphous silica demonstrated some chemotactic effect on HUVECs, observations that match with a previous publication.[22] Among the amorphous silica-coated implant groups, SiONP2 presented the largest improvement in cell migration, which can be attributed to the presence of ionic P or due to the different surface composition of Si, O, and N observed on SiONP1 and SiONP2 implants, as shown in Table 1. We observed that SIONP2 implant's surface has two times more oxygen than the SiONP1 group, and this difference can illustrate the enhancement in HUVECs angiogenesis in the SiONP2 group.

The analysis of fibronectin deposition after 5 days showed that the amount of fibronectin was markedly increased in the SiONP2 group, which can be attributed not just to the effect of the surface chemistry, but to the higher surface energy observed on the SiONP2 group demonstrated by the lowest contact angle (Fig. 1). Fibronectin is a extracellular glycoprotein produced by endothelial cells in the early stages of new blood vessel formation.[47,48] The presence of this protein is important for endothelial cell differentiation, migration, and proliferation.[47–50] Therefore, its presence can be used as a demonstration of an efficient HUVECs matrix deposition.[48] Our results demonstrate that SiON, SiONP1, and SiONP2 (Figs. 4E–J) formed a circular structure matrix deposition, similar to the capillary tubule formation, and the SiONP2 group showed a significant enhanced deposition (Fig. 4J).

The capillary tubule formation assay on a bed of Matrigel used TCP and EGM-2 as the positive control, and as expected, the TCP presented the largest capillary network structure (Fig. 5B, F). The other groups: negative control (GCS) and amorphous silica-coated implants were supplemented with 2% FBS and 1% P/S without the growth factors present on EGM-2. As we can observe on fluorescent images (Fig. 5D, E, and G), the tubule thickness was enhanced in the SiONP groups. Moreover, the total tubule length was significantly increased in the SiON and SiONP groups compared with the GCS, which can be attributed to the high surface energy (low contact angle) and the surface chemistry.

The above results confirm the previous results showing that silica-based materials can improve capillary tubule length in HUVECs and give more insight on the effect of those materials on capillary tube thickness that was not analyzed before.[44]

In addition, the gene expression of angiogenic markers study showed a significant upregulation of *VEGF-A*, *HIF-1α*, *Ang-1*, and *Nesp-2* on HUVECs on SiON and SiONP implants. *VEGF-A* is a major angiogenesis regulator that binds and activates the *VEGF* receptor inducing endothelial cell proliferation, migration, and capillary tubule formation. A recent publication verified the crucial role of ionic Si on angiogenesis by upregulating *HIF-1α* and inducing angiogenesis in endothelial cells.[44] Some studies showed that P can upregulate *VEGF-A* and induces endothelial cell migration and proliferation.[30,31,46]

Ang-1 is a protein produced by endothelial cells that can induce HUVECs migration and differentiation.[37] Moreover, by activation of the tyrosine kinase 2 (*Tie2*-receptor) can protect endothelial cells under unfavorable survival conditions against apoptosis.[38,51] *Nes-2* is an intracellular protein that connects the actin filament to the endothelial cell nuclei and has been related with endothelial cell shape changing and migration.[52] As we could verify the upregulation of *Nes-2* in our samples coated with amorphous silica by PECVD, we believe that *Nes-2* could have some relationship with the enhancement in a capillary tubule formation network and transwell cell migration observed mainly on the SiONP1 and SiONP2 groups.

By correlating the upregulation of these angiogenic markers to the chemical structure of each coating, it was found that as the phosphate to nitrogen ratio increased in the coating (P/N = 0.0, 0.9, and 1.0 for SiON, SiONP1, and SiONP2, respectively), angiogenic marker expression increased. This can be attributed to the change in surface coordination or surface functional group formation and its impact on cell response. These findings can be supported by previous publications that showed the importance of ionic phosphorous on protein kinase B (*Akt*) activation.[28,29] The *Akt* pathway downstream induces *HIF-1α* and *Ang-1* synthesis[53,54] that are essential for endothelial cell survival, growth, proliferation, and migration.[55,56]

Another study also noted that extracellular inorganic phosphate activated the *Akt* pathway by suppressing levels of membrane-bound phosphatases and tensin homolog.[57] Moreover, it is well known that *HIF-1α* is a transcription factor of *VEGF-A*.[58] Thus, in the current study, we suggest that the inorganic phosphate from SiONP coatings upregulated *HIF-1α*, *Ang-1* and *VEGF-A* through the *Akt* signaling pathway (sodium-dependent phosphate cotransporter, NPT). This pathway is regulated by the concentration of inorganic phosphate and as such may have improved endothelial cell viability, proliferation, migration, and capillary tubule formation.

We also analyzed the gene expression of oxidative stress markers. We observed the upregulation of enzymes that play a major role in the catalysis of reactive oxygen species and

its products. *SOD-1* and *cat-1* were significantly upregulated in cells exposed to SiON, SiONP1, and SiONP2 implants compared with the control group, especially at the first 24 h. At 24 h, SiONP2 implants presented a remarkable *cat-1* upregulation among all studied groups showing threefold more mRNA than the control.

In a recent publication, our group demonstrated the relevant role of ionic Si on *SOD-1* upregulation in osteoblasts.[17] There are few studies that indicate the correlation of the effect of ionic Si or silica base materials with endothelial cells and antioxidant enzymes. *SOD-1* is an enzyme that catalyze the conversion of O_2^- (superoxide) in H_2O_2.[59,60] *Cat-1* is an enzyme responsible for catalyzing the conversion H_2O_2 in H_2O and O_2.[61,62] These enzymes play a major role during physiological and pathological oxidative stress conditions where H_2O_2 and O_2^- are the main reactive oxygen species produced by cells under oxidative stress. Further investigations are necessary for a better understanding of a possible antioxidant effect of these biomaterials on HUVECs.

Conclusions

Our present study demonstrated that PECVD-coated amorphous silica-based materials formed by Si, O, N, and P can successfully enhance the angiogenic properties of HUVECs, improving cell proliferation, migration, fibronectin deposition, and capillary tubule formation by upregulating *VEGF-A*, *HIF-1α, nesprin-2*, and *Ang-1*. The angiogenic enhancement by these implants may induce faster osteointegration and healing, preventing complications such as implants loosening and failure. Additionally, *Cat-1* and *SOD-1* upregulation open some doors for further investigations of a possible antioxidant effect of these implants, which could be beneficial for improving the osteointegration and healing in the unfavorable oxidative stress environment of large bone defects.

Acknowledgments

The authors would like to thank Olumide Aruwajoye, Suresh Adapala, Ila Oxendine, Yang Li, Reuel Cornelia, and Richard Banlaygas from the Center for Excellence in Hip Disorders, Texas Scottish Rite Hospital, and Ami Shah from UTA, for their assistance. We would like to thank the Brazilian Federal Government, Coordenacao de Aperfeicoamento de Pessoal de Nivel Superior (CAPES), for sponsoring the first author. We also would like to thank the Fulbright scholarships program and the National Research Centre at Egypt for sponsoring the second author. This work was supported by a grant from the National Institutes of Health (1R03DE023872-01A1) to V.G.V. and was partially supported by Departmental Startup (#304-128170, V.G.V., PI) and Enhancement Grant (#24444100005, V.G.V., PI). We would like to thank the NIH/NIDCR for their support on this project (Grant #1R56DE027964-01A1).

Disclosure Statement

No competing financial interests exist.

References

1. Saran, U., Piperni, S.G., and Chatterjee, S. Role of angiogenesis in bone repair. Arch Biochem Biophys **561,** 109, 2014.
2. Wiese, A., and Pape, H.C. Bone defects caused by high-energy injuries, bone loss, infected nonunions, and nonunions. Orthop Clin North Am **41,** 1–4, table of contents 2010.
3. Filipowska, J., *et al.* The role of vasculature in bone development, regeneration and proper systemic functioning. Angiogenesis **20,** 291, 2017.
4. Höhne, J., *et al.* Outcomes of cranioplasty with preformed titanium versus freehand molded polymethylmethacrylate implants. J Neurol Surg Part A Cent Eur Neurosurg **79,** 200, 2018.
5. Bone fracture healing: cell therapy in delayed unions and nonunions. Bone **70,** 93, 2015.
6. Zanotti, B., *et al.* Cranioplasty: review of materials. J Craniofac Surg **27,** 2061, 2016.
7. Parthasarathy, J. 3D modeling, custom implants and its future perspectives in craniofacial surgery. Ann Maxillofac Surg **4,** 9, 2014.
8. Merolli, A., *et al.* Debris of carbon-fibers originated from a CFRP (pEEK) wrist-plate triggered a destruent synovitis in human. J Mater Sci Mater Med **27,** 50 2016.
9. Stratton-Powell, A.A., Pasko, K.M., Brockett, C.L., and Tipper, J.L. The biologic response to polyetheretherketone (PEEK) wear particles in total joint replacement: a systematic review. Clin Orthop Relat Res **474,** 2394, 2016.
10. Lethaus, B., Bloebaum, M., Koper, D., Poort-Ter Laak, M., and Kessler, P. Interval cranioplasty with patient-specific implants and autogenous bone grafts e Success and cost analysis. J Cranio-Maxillofacial Surg **42,** 1948, 2014.
11. Say, Y., and Aksakal, B. Effects of hydroxyapatite/Zr and bioglass/Zr coatings on morphology and corrosion behaviour of Rex-734 alloy. J Mater Sci Mater Med **27,** 105 2016.
12. Popa, A.-C., *et al.* Bioglass implant-coating interactions in synthetic physiological fluids with varying degrees of biomimicry. Int J Nanomedicine **12,** 683, 2017.
13. Camilo, C.C., *et al.* Bone response to porous alumina implants coated with bioactive materials, observed using different characterization techniques. J Appl Biomater Funct Mater **15,** e223, 2017.
14. Hoornenborg, D., *et al.* Does hydroxyapatite coating enhance ingrowth and improve longevity of a Zweymuller type stem? A double-blinded randomised RSA trial. Hip Int **28,** 115, 2017.
15. Yuan, H., de Bruijn, J.D., Zhang, X., van Blitterswijk, C.A., and de Groot, K. Bone induction by porous glass ceramic made from Bioglass (45S5). J Biomed Mater Res **58,** 270, 2001.
16. Pavón, J., Jiménez-Piqué, E., Anglada, M., Saiz, E., and Tomsia, A.P. Delamination under Hertzian cyclic loading of a glass coating on Ti6al4v for implants. J Mater Sci **41,** 5145, 2006.
17. Ilyas, A., *et al.* Amorphous Silica: a new antioxidant role for rapid critical-sized bone defect healing. Adv Healthc Mater **5,** 2199, 2016.
18. Saffarian Tousi, N., *et al.* Combinatorial effect of Si4 +, Ca2 +, and Mg 2 + released from bioactive glasses on osteoblast osteocalcin expression and biomineralization. Mater Sci Eng C **33,** 2757, 2013.
19. Varanasi, V.G., *et al.* Si and Ca individually and combinatorially target enhanced MC3T3-E1 subclone 4 early osteogenic marker expression. J Oral Implantol **38,** 325, 2012.

20. Odatsu, T., *et al.* Human periosteum cell osteogenic differentiation enhanced by ionic silicon release from porous amorphous silica fibrous scaffolds. J Biomed Mater Res Part A **103,** 2797, 2015.
21. Ilyas, A., Lavrik, N.V., Kim, H.K.W., Aswath, P.B., and Varanasi, V.G. Enhanced interfacial adhesion and osteogenesis for rapid "bone-like" biomineralization by PECVD-based silicon oxynitride overlays. ACS Appl Mater Interfaces **7,** 15368, 2015.
22. Dashnyam, K., *et al.* Promoting angiogenesis with mesoporous microcarriers through a synergistic action of delivered silicon ion and VEGF. Biomaterials **116,** 145, 2017.
23. Varanasi, V.G., *et al.* Role of hydrogen and nitrogen on the surface chemical structure of bioactive amorphous Silicon oxynitride films. J Phys Chem B **121,** 8991, 2017.
24. Kim, S.H., *et al.* Correlation of proliferation, morphology and biological responses of fibroblasts on LDPE with different surface wettability. J Biomater Sci Polym Ed **18,** 609, 2007.
25. Raimondo, T., Puckett, S., and Webster, T.J. Greater osteoblast and endothelial cell adhesion on nanostructured polyethylene and titanium. Int J Nanomed **5,** 647, 2010.
26. Chai, F., *et al.* Improving endothelial cell adhesion and proliferation on titanium by sol-gel derived oxide coating. J Biomed Mater Res A **92,** 754, 2010.
27. Arima, Y., and Iwata, H. Effect of wettability and surface functional groups on protein adsorption and cell adhesion using well-defined mixed self-assembled monolayers. Biomaterials **28,** 3074, 2007.
28. Chang, S.H., *et al.* Elevated inorganic phosphate stimulates Akt ERK1/2-Mnk1 signaling in human lung cells. Am J Respir Cell Mol Biol **35,** 528, 2006.
29. Jin, H., *et al.* High dietary inorganic phosphate affects lung through altering protein translation, cell cycle, and angiogenesis in developing mice. Toxicol Sci **100,** 215, 2007.
30. Camalier, C.E., *et al.* An integrated understanding of the physiological response to elevated extracellular phosphate. J Cell Physiol **228,** 1536, 2013.
31. Saghiri, M.A., Asatourian, A., Orangi, J., Sorenson, C.M., and Sheibani, N. Functional role of inorganic trace elements in angiogenesis—Part I: N, Fe, Se, P, Au, and Ca. Crit Rev Oncol **96,** 129, 2015.
32. Matsunaga, T., *et al.* Angiostatin inhibits coronary angiogenesis during impaired production of nitric oxide. Circulation **105,** 2185, 2002.
33. Förstermann, U., and Sessa, W.C. Nitric oxide synthases: regulation and function. Eur Heart J **33,** 829, 837a, 2012.
34. Morbidelli, L., Donnini, S., and Ziche, M. Role of nitric oxide in the modulation of angiogenesis. Curr Pharm Des **9,** 521, 2003.
35. Dimmeler, S., and Zeiher, A.M. Nitric oxide-an endothelial cell survival factor. Cell Death Differ **6,** 964, 1999.
36. Lee, P.C., *et al.* Nitric oxide induces angiogenesis and upregulates αvβ3 integrin expression on endothelial cells. Microvasc Res **60,** 269, 2000.
37. Harel, S., Mayaki, D., Sanchez, V., and Hussain, S.N.A. NOX2, NOX4, and mitochondrial-derived reactive oxygen species contribute to angiopoietin-1 signaling and angiogenic responses in endothelial cells. Vasc Pharmacol **92**, 22, 2017.
38. Jin Kwak, H., So, J.-N., Jae Lee, S., Kim, I., and Young Koh, G. Angiopoietin-1 is an apoptosis survival factor for endothelial cells. Fed Eur Biochem Soc **448**, 249, 1999.
39. Ilyas, A., *et al.* Rapid regeneration of vascularized bone by nanofabricated amorphous Silicon. J Biomed Nanotechnol **15,** 1, 2019.
40. Zhang, Y., *et al.* Mesoporous bioactive glass nanolayer-functionalized 3D-printed scaffolds for accelerating osteogenesis and angiogenesis. Nanoscale **7,** 19207, 2015.
41. Chaiwong, S. S., *et al.* Wettability effect of PECVD-SiO x films on Poly(lactic acid) induced by oxygen plasma on protein adsorption and cell attachment. J Phys Conf Ser **423,** 12042, 2013.
42. Terriza, A., *et al.* Osteoblasts interaction with PLGA membranes functionalized with titanium film nanolayer by PECVD. In vitro assessment of surface influence on cell adhesion during initial cell to material interaction. Materials (Basel) **7,** 1687, 2014.
43. Surmeneva, M.A., *et al.* Nano-hydroxyapatite-coated metal-ceramic composite of iron-tricalcium phosphate: Improving the surface wettability, adhesion and proliferation of mesenchymal stem cells *in vitro*. Colloids Surfaces B Biointerfaces **135,** 386, 2015.
44. Dashnyam, K., *et al.* A mini review focused on the proangiogenic role of silicate ions released from silicon-containing biomaterials. J Tissue Eng **8,** 204173141770733, 2017.
45. Lin, Y., Mckinnon, K.E., Ha, S.W., and Beck, G.R. Inorganic phosphate induces cancer cell mediated angiogenesis dependent on forkhead box protein C2 (FOXC2) regulated osteopontin expression. Mol Carcinog **54,** 926, 2015.
46. Hielscher, A., Ellis, K., Qiu, C., Porterfield, J., and Gerecht, S. Fibronectin deposition participates in extracellular matrix assembly and vascular morphogenesis. PLoS One **11,** 1, 2016.
47. Chiang, H.Y., Korshunov, V.A., Serour, A., Shi, F., and Sottile, J. Fibronectin is an important regulator of flow-induced vascular remodeling. Arterioscler Thromb Vasc Biol **29,** 1074, 2009.
48. Kusuma, S., Zhao, S., and Gerecht, S. The extracellular matrix is a novel attribute of endothelial progenitors and of hypoxic mature endothelial cells. FASEB J **26,** 4925, 2012.
49. Salakhutdinov, I., *et al.* Fibronectin adsorption to nanopatterned silicon surfaces. J Nanomater **2008,** 5, 2008.
50. Harfouche, R., *et al.* Mechanisms which mediate the anti-apoptotic effects of angiopoietin-1 on endothelial cells. Microvasc Res **64,** 135, 2002.
51. King, S.J., *et al.* Nesprin-1 and nesprin-2 regulate endothelial cell shape and migration. Cytoskeleton **71,** 423, 2014.
52. Harada, H., *et al.* The Akt/mTOR pathway assures the synthesis of HIF-1α protein in a glucose- and reoxygenation-dependent manner in irradiated tumors. J Biol Chem **284,** 5332, 2009.
53. Huang, J.J., *et al.* Angiogenesis effect of therapeutic ultrasound on HUVECs through activation of the PI3K-Akt-eNOS signal pathway. Am J Transl Res **7,** 1106, 2015.
54. Somanath, P.R., Razorenova, O.V., Chen, J., and Byzova, T.V. Akt1 in endothelial cell and angiogenesis. Cell Cycle **5,** 512, 2006.
55. Lee, M.Y., *et al.* Endothelial Akt1 mediates angiogenesis by phosphorylating multiple angiogenic substrates. Proc Natl Acad Sci **111,** 12865, 2014.
56. Kawai, M., Kinoshita, S., Ozono, K., and Michigami, T. Inorganic phosphate activates the AKT/mTORC1 pathway

and shortens the life span of an -Klotho-deficient model. J Am Soc Nephrol **27,** 2810, 2016.
57. Conway, E.M., Collen, D., and Carmeliet, P. Molecular mechanisms of blood vessel growth. Cardiovasc Res **49,** 507, 2001.
58. Choi, Y.J., Lee, J.Y., Chung, C.P., and Park, Y.J. Cell-penetrating superoxide dismutase attenuates oxidative stress-induced senescence by regulating the p53-p21 (Cip1) pathway and restores osteoblastic differentiation in human dental pulp stem cells. Int J Nanomed **7,** 5091, 2012.
59. Fukai, T., and Ushio-Fukai, M. Superoxide dismutases: role in redox signaling, vascular function, and diseases. Antioxid Redox Signal **15,** 1583, 2011.
60. Chelikani, P., Fita, I., and Loewen, P.C. Diversity of structures and properties among catalases. Cell Mol Life Sci **61,** 192, 2004.
61. Fernández, C., San Miguel, E. and Fernández-Briera, A. Superoxide dismutase and catalase: tissue activities and relation with age in the long-lived species Margaritifera margaritifera. Biol Res **42,** 57, 2009.
62. Saxena, S., and Jamil, K. Oxidative stress and expression level of Catalase, Glutathione S Tranferase Enzyme in type 2 Diabetes Patients. Int J Sci Eng Res **5,** 1127, 2014.

Address correspondence to:
Venu G. Varanasi, PhD
Bone-Muscle Research Center
College of Nursing and Health Innovation
University of Texas at Arlington
411 S. Nedderman Drive
Arlington, TX 76019-0407

E-mail: venu.varanasi@uta.edu

Received: February 13, 2019
Accepted: April 29, 2019
Online Publication Date: August 23, 2019